Neoproterozoic Re-Os systematics of organic-rich rocks in the São Francisco Basin, Brazil and implications for hydrocarbon exploration

Maria E. Bertoni[a*], Alan D. Rooney[b,c], David Selby[b], Fernando F. Alkmim[d], Daniel P. Le Heron[a]

[a]Department of Earth Sciences, Queen's Building, Royal Holloway University of London, Egham, Surrey, TW20 0BY, UK

[b]Department of Earth Sciences, Durham University, Durham, DH1 3LE, UK.

[c]Department of Earth and Planetary Sciences, Harvard University, Cambridge, MA, 02138, USA

[d]Departamento de Geologia, Escola de Minas, Universidade Federal de Ouro Preto, Morro do Cruzeiro, 35.400.000 Ouro Preto, MG, Brazil

Abstract

The São Francisco Basin contains a remarkable archive of Neoproterozoic strata and its hydrocarbon-bearing strata are receiving increasing attention as global oil and gas exploration targets progressively deeper and older rocks. New Re–Os geochronology for the Paracatu Slate Formation of the Canastra Group, Brazil yields a depositional age of 1002 ± 45 Ma. This age represents the first successful application of the Re–Os system to rocks of this group and indicates excellent agreement with a previously

published U–Pb detrital zircon age (Rodrigues et al., 2010). Together with TOC values of ca. 2 wt.% (despite greenschist metamorphism), it might be argued that the São Francisco Basin has had the potential for hydrocarbon generation since the Tonian (1000 – 850 Ma). In addition, we also report an imprecise Re–Os age (1304 ± 210 Ma) for the Serra do Garrote Formation, a further potential source rock of the Vazante Group. We suggest, based on petrological evidence, that the Re–Os systematics were disturbed by post-depositional fluid flow that was most likely associated with Vazante ore deposit mineralization. An attempt to determine a Re-Os date for the Sete Lagoas Formation, a putative post-Sturtian cap carbonate, is precluded owing to low Re abundances (≤100 ppt). Major environmental changes in the aftermath of the Jequitaí glaciation, particularly the development of palaeotopography such as subglacial tunnel valleys, may account for the apparent random distribution of TOC enrichment in these Cryogenian/Ediacaran post-glacial deposits. This scenario might thus have major implications for the hydrocarbon prospectivity of this post-glacial succession.

Keywords: Re–Os, Neoproterozoic, Canastra, Vazante, Bambuí, source rock

*Corresponding author. Tel: +44 (0) 1784 443 581. Postal address: Department of Earth Sciences, Royal Holloway University of London, Egham Hill, Egham, Surrey, TW20 0EX, UK. E-mail addresses: maria.bertoni.2009@live.rhul.ac.uk, bertonime@gmail.com. (M. E. Bertoni)

1. Introduction

The São Francisco Basin and its surrounding belts contain an extensive stratigraphic archive of Proterozoic time, extending at least from the Statherian (1750 Ma) to Late Ediacaran (560 Ma) (Alkmim and Martins-Neto, 2012; Paula-Santos, 2013; Warren et al., 2014). Over a wide area, diamictites and associated cap carbonates have been correlated and linked to major Earth events, as the Sturtian (Babinski and Kaufman, 2003; Azmy et al., 2006; Babinski et al., 2007; Vieira et al., 2007) and Marinoan (Caxito et al., 2012) glacial epochs. In addition, the São Francisco Basin has multiple hydrocarbon gas shows, which are probably sourced from Meso-Neoproterozoic organic-rich rocks (Craig et al., 2013 and references therein). However, the lack of accurate geochronological data throughout the stratigraphy hinders attempts to develop a chronological framework for the São Francisco Basin and its surrounding belts. An understanding of the hydrocarbon potential of these rocks and the relationship of organic-rich horizons to global geological events requires a precise geochronological framework. The absence of volcanic ash layers for U-Pb and Ar-Ar geochronology has hindered attempts to gain absolute geochronological age data (Misi et al., 2011). In addition, age control in these strata is further hampered by the general lack of biostratigraphic constraints, intense deformation and metamorphism. Placing accurate geochronological constraints on organic-rich horizons is integral to understanding of the nature of the depositional environment and fossil hydrocarbon system in this vast basin.

The rhenium–osmium (Re–Os) geochronometer is an increasingly recognized tool for determining depositional ages of organic-rich rocks (Ravizza and Turekian, 1989; Cohen et al., 1999; Selby and Creaser, 2005a; Georgiev et al., 2011; van Acken

et al., 2013) and hydrocarbon deposits (Selby et al., 2005; Selby and Creaser, 2005b). The method has yielded absolute dates for Neoproterozoic strata with precision approaching 0.5 % uncertainty (2σ) in units up to greenschist facies (Kendall et al., 2004; Rooney et al., 2014). In the São Francisco Basin of Brazil (**Fig. 1A**) the Re-Os radioisotope system has been previously utilized with limited success to provide depositional ages for the Vazante Group (Geboy, 2006; Azmy et al., 2008; Geboy et al., 2013). Here we evaluate and discuss Re-Os geochronology of the Canastra, Vazante and Bambuí groups with the aim of constraining the depositional age of the organic-rich strata of the Paracatu, Serra do Garrote and Sete Lagoas formations. More widely, this study contributes to the radiometric calibration of the Proterozoic rock record in Brazil, and hence to a better understanding of the geological evolution of the Brasília Belt and São Francisco Basin.

2. Geological setting and existing chronostratigraphy

The São Francisco Craton (**Fig. 1A**) is one of the oldest portions of the Precambrian nucleus of South America (Almeida et al., 2000). Together with the other cratons of South America, it represents the internal portions of plates involved in the assembly of West Gondwana toward the end of the Proterozoic Era (Alkmim and Martins-Neto, 2012). The Brasiliano/Pan-African Orogenic Belts, meanwhile, fringe those ancient plates and also include marginal metasediments accreted during collision (Almeida et al., 2000; Alkmim et al., 2001; Alkmim and Martins-Neto, 2012). The Brasilia Belt, which flanks the São Francisco Basin to the west, exhibits a fundamentally complex tectonic character and variable metamorphic grade. Therefore, it is essential to briefly outline the structural character, the stratigraphy, and present geochronology of both the Brasília Belt and the São Francisco Basin.

"Insert Figure 1 here"

2.1 The Brasilia Belt and São Francisco Basin

The Brasilia Belt, located on the western margin of the São Francisco Craton (**Fig. 1B**), is the product of a collision between the Amazon, São Francisco-Congo and Paranapanema paleocontinents (ca. 850-550 Ma; Pimentel et al., 1999) during the amalgamation of Gondwana (Li et al., 2008; Pimentel et al., 2011; Rodrigues et al., 2012). This belt is composed of thrust sheets verging eastward towards the São Francisco platform (**Fig. 1B**). Metamorphic grade increases progressively westward, reaching granulite facies conditions in the central part of the belt (Dardenne, 2000).

The southern Brasília Belt involves sedimentary rocks grouped into several lithostratigraphic units (**Fig. 1B**): the Araxá, Paranoá, Canastra, and Ibiá groups (Pimentel et al., 2011). Intense deformation, the lack of intercalated volcanic horizons, and the absence of biostratigraphic controls results in multiple possible interpretations for this supracrustal succession (Dardenne, 2000; Valeriano et al., 2008; and references therein). Provenance studies suggest that the Paranoá and Canastra groups are passive margin deposits of the São Francisco paleocontinent, while the Araxá, and Ibiá groups are synorogenic (fore- or back-arc) basin fill (Pimentel et al., 2001; Rodrigues et al., 2010; Pimentel et al., 2011).

The São Francisco Basin occupies the ca. 800 km-long NS-trending lobe of the São Francisco Craton (**Fig. 1A**). Bounded to the west and to the east by emergent thrusts of the adjacent Brasília and Araçuaí Orogenic Belts respectively, the basin is filled by Palaeo-Mesoproterozoic units (Espinhaço Supergroup and Paranoá Group),

123 and Meso-Neoproterozoic strata of the Vazante Group, Jequitaí Formation, and
124 Bambuí Group (Alkmim and Martins-Neto, 2012).
125
126 *2.2 Canastra Group*
127 The Canastra Group subdivides into three formations (Serra do Landim, Paracatu and
128 Serra dos Pilões). These rocks, which are mainly present in the southern portion of the
129 eastern Brasilia Orogen (**Fig. 1B**), comprise phyllite and quartzite with common
130 carbonate beds (Pereira et al., 1994; Dias, 2011). These have experienced lower
131 greenschist (2-3 kbar and 350-380 °C) facies metamorphism (Freitas-Silva, 1996;
132 Dardenne, 2000). Thrust contacts characterize the boundaries between the Canastra
133 and lower grade metamorphic strata of the Vazante, Paranoá and Bambuí groups
134 (Pereira et al., 1994). It has been suggested that the Canastra Group is a lateral
135 equivalent of the Paranoá Group (Dardenne, 2000; Pimentel et al., 2011).
136 The lithostratigraphy of the Canastra Group is difficult to unravel owing to
137 numerous thrust faults (Rodrigues et al., 2010) (**Fig. 2**), especially for the basal Serra
138 do Landim Formation (chlorite-rich calc-phyllite and calcschist) and the upper units
139 (Paracatu and the Chapada dos Pilões formations). The Paracatu Formation, which
140 can reach up to ca. 2500 m in thickness (Dias, 2011) comprises slope turbidites and
141 basinal, carbonaceous phyllites rich in diagenetic pyrite, whereas the Chapada dos
142 Pilões Formation consists of shallow marine wave and storm-influenced clastics
143 (Pereira et al., 1994). The coarsening upward succession in the upper Canastra Group
144 thus records a regressive continental platform megasequence (Pereira et al., 1994).
145 For the Canastra Group, detrital zircon ages reveal Paleoproterozoic (ca. 1.8
146 and 2.1 Ga) and Mesoproterozoic (1.1-1.2 Ga) peaks, particularly for the Paracatu
147 Formation (Rodrigues et al., 2010). The absence of Neoproterozoic zircon grains

148 related to the active margin of the Brasília Belt, in addition to homogeneous
149 Paleoproterozoic Sm–Nd model ages (ca. 2.2 Ga) (Pimentel et al., 2001) suggests the
150 São Francisco-Congo Craton as the main source region. This led to the interpretation
151 of the Canastra Group as a passive margin succession (Pimentel et al., 2001, 2011).
152 The youngest detrital zircons in the Paracatu Formation are ca. 1040 Ma (Valeriano et
153 al., 2004; Rodrigues et al., 2010; Dias, 2011) (**Fig. 2**); the origin of the
154 Mesoproterozoic (ca. 1.2 Ga) population remains uncertain.
155 The diagenetic age of the ore-hosting carbonaceous phyllites of the Morro do
156 Ouro Member of the Paracatu Formation has been estimated at 1000-1300 Ma based
157 on Rb-Sr and K-Ar chlorite, and Pb-Pb galena ages (Freitas-Silva, 1996).
158 Metamorphism and gold enrichment of this unit is related to the Brasiliano Event at
159 ca. 680 Ma (Freitas-Silva, 1996).
160
161 "Insert Figure 2 here"
162
163 *2.3 Vazante Group*
164 The Vazante Group positioned in the western margin of the São Francisco Basin (**Fig.**
165 **1B**), comprises thick (ca. 5000 m) siliciclastic-dolomite (**Fig. 3**) of marine origin
166 (Azmy et al., 2008; Misi et al., 2011). The Vazante Group is divided into seven
167 formations (Santo Antonio do Bonito, Rocinha, Lagamar, Serra do Garrote, Serra do
168 Poço Verde, Morro do Calcário and Lapa; Dardenne, 2000), which experienced
169 greenschist facies metamorphism. Neoproterozoic Brasiliano thrusts and nappes
170 obscure many sedimentary contacts (Dardenne, 2000), particularly with the Canastra
171 Group to the west and the Bambuí Group to the east (Rodrigues et al., 2012). Intense
172 deformation in the outcrop area raises major uncertainties about the internal

173 stratigraphy and lateral correlation of the units.

174 In this paper, we analyzed the Serra do Garrote Formation (**Fig. 3**). This
175 formation, which can reach up to 1000 m in thickness (Misi et al., 2011), is
176 dominantly carbonaceous and pyrite-bearing slate, intercalated with fine quartzite
177 beds, representing an open marine succession deposited below storm wave base
178 (Madalosso, 1980). The Serra do Poço Verde Formation lies conformably over the
179 Serra do Garrote Formation and is dominantly dolomitic. The presence of glendonite
180 pseudomorphs after ikaite and dropstones in slates was interpreted as suggestive of
181 paraglacial depositional conditions (Olcott et al., 2005). The Morro do Calcário
182 Formation, a carbonate-stromatolitic succession, often diamictitic (Dardenne, 2000),
183 conformably overlies the former unit. The Morro do Calcário Formation is truncated
184 by an unconformity at the base of the overlying Lapa Formation (Misi et al., 2005),
185 which contains diamictites, organic-rich shale, and cap carbonates with a
186 characteristic negative $\delta^{13}C_{carbonate}$ excursion (ca. -8 to 0 ‰) interpreted to record the
187 resumption of primary productivity in the aftermath of glaciation (Azmy et al., 2006;
188 2008). A reassessment of the core used by Azmy et al. (2006, 2008) concluded that
189 the unit is part of the Morro do Calcário Formation rather than the Lapa Formation as
190 previously thought (Geboy et al., 2013).

191 Based on C and Sr isotope profiles, the Morro do Calcário Formation is
192 correlated with the Sturtian glacial epoch (Azmy et al., 2006; ca. 717 Ma; Macdonald
193 et al., 2010). Globally, the chronometry of the Sturtian glaciation is considered to
194 encompass a ca. 60 Myr window, based on U-Pb zircon and Re-Os geochronology of
195 syn- and post-glacial deposits associated with the Rapitan glacial succession in NW
196 Canada (Macdonald et al., 2010; Rooney et al., 2014). However, Re-Os analyses yield
197 Mesoproterozoic depositional ages for organic-rich shales of the Serra do Garrote

198 (1353 ± 69 Ma) and Serra do Poço Verde (1126 ± 47 Ma) formations, respectively
199 (**Fig. 3**). The same technique together with U-Pb measurements on detrital zircons of
200 the Morro do Calcário Formation, suggest deposition at ca. 1000–1100 Ma (Azmy et
201 al., 2008; **Fig. 3**). As a result, the Vazante Group is considered late Mesoproterozoic,
202 rather than Sturtian (Azmy et al., 2008). Additional, SHRIMP U–Pb detrital zircon
203 analyses (Rodrigues et al., 2012) of five formations of the Vazante Group has
204 identified the youngest population ages (ca. 930 Ma) at the base of the group, and
205 older populations (ranging ca. 1200-1000 Ma) toward the top (**Fig. 3**). A reverse fault
206 identified between the Rocinha and Lagamar formations solve the paradoxical
207 stratigraphic age inversion (Geboy et al., 2013). The same authors also present Re-Os
208 ages for the Serra do Garrote and Morro do Calcário formations of 1354 ± 88 Ma and
209 1112 ± 50 Ma, respectively (**Fig. 3**).
210 Despite the complex history of the Vazante Group, the detrital zircon age
211 pattern of the Serra do Garrote Formation (ca. 1.29 Ga, Rodrigues et al., 2012) is
212 coherent with Re-Os isochron ages obtained for the same formation (ca. 1.35 Ga,
213 Geboy, 2006; Geboy et al., 2013). However, high Mean Square of Weighted Deviates
214 (MSWD) values of 26 and 49 is associated with these Re-Os isochrons rendering
215 them imprecise and less than conclusive with regards to the true age of the Vazante
216 Group (Geboy, 2006; Geboy et al., 2013). Therefore, further provision of radiometric
217 ages is clearly necessary, and motivates our attempts to date the Serra do Garrote
218 Formation.
219
220 "Insert Figure 3 here"
221
222 *2.4 Neoproterozoic glacials and the Jequitaí Formation*

223 Evidence for glaciation in the Jequitaí Formation in the São Francisco Basin and its
224 correlatives, the Bebedouro Formation (northern São Francisco Craton) and
225 Macaúbas Group (Araçuaí Belt), is compelling (e.g. Cukrov et al., 2005; Uhlein et al.,
226 2007; Chaves et al., 2010). The preceding authors reported a striated pavement cut
227 into the Espinhaço Supergroup in the northeastern portion of the São Francisco Basin,
228 together with abundant diamictites with exotic lonestones, some of which are well
229 stratified and exhibit unequivocal impact structures implying ice-rafted debris.
230 Furthermore, on the western margin of the São Francisco Basin, Martins-Ferreira et
231 al. (2013; **Fig. 1**) describe a ca. 4 km-wide valley carved in sandstone of the Paranoá
232 Group and filled by a ca. 40 m package of sandstone, diamictite and tillite of the
233 Jequitaí Formation. These glaciogenic rocks are, in turn, covered by a cap carbonate
234 that marks the base of the Bambuí Group in the São Francisco Basin (**Fig. 4**). With
235 the exception of the striated pavement, each of these facies are recognised in
236 proprietary cores across the subsurface of the basin. Zircons U-Pb systematics
237 extracted from the Jequitaí Formation and the correlative Macaúbas Group yield
238 maximum deposition ages of 880 Ma and 864 Ma, respectively (Pedrosa-Soares et al.,
239 2000; Rodrigues et al., 2008).
240
241 *2.5 Bambuí Group*
242 These epicontinental deposits, of alternating siliciclastics and carbonates are the most
243 widely distributed unit in the São Francisco Basin (**Fig. 1**), draping the Jequitaí
244 diamictites and sandstones. They form a shallowing upwards sequence (Dardenne,
245 2000; Santos et al., 2000), divisible into three coarsening upward megacycles
246 (Dardenne, 2000; Martins-Neto, 2009). The first megacycle is represented by the Sete
247 Lagoas Formation, the second includes the Serra de Santa Helena and Lagoa do

248 Jacaré formations and the last cycle comprises the Serra da Saudade and Três Marias
249 formations (Martins and Lemos, 2007) (**Fig. 4**). The absence of volcanic ash horizons
250 throughout the Bambuí Group, in addition to hampering geochronology, has
251 promoted debate regarding the tectonic setting for this group (e.g. Alkmim and
252 Martins-Neto, 2001; Zalán and Silva, 2007) and its relationship with the Jequitaí
253 diamictites (Babinski et al., 2007, 2012; Misi et al., 2011; Caxito et al., 2012).

254 The Sete Lagoas Formation, for which we present data in this paper,
255 comprises a ca. 200 m succession (Vieira et al., 2007) of siliciclastic-calcareous
256 sediments, grading upwards into microcrystalline limestones and dolostones. Its upper
257 section contains the most extensive shallow water carbonates of the basin with
258 laminated and columnar *Gymnosolenide* stromatolites (Dardenne, 1978) and evidence
259 for subaerial exposure (Martins and Lemos 2007). Its basal contact is characterized by
260 an unconformity: the formation rests on granite-gneiss basement, on the glaciogenic
261 Jequitaí Formation, or on conglomerates of the Carrancas Formation, exposed along
262 the southern border of the basin (Dardenne, 2000, Alkmin and Martins-Neto, 2001,
263 Vieira et al., 2007).

264 Several isotopic studies have demonstrated a negative excursion of $\delta^{13}C_{carbonate}$
265 (ca. -4 to 0 ‰) for the base of the Sete Lagoas Formation (e.g. Alvarenga et al., 2007;
266 Kuchenbecker, 2011). The $\delta^{13}C$ signature, together with its stratigraphic position,
267 sitting on top of the Jequitaí diamictite deposits, has led to interpretations of a typical
268 postglacial cap carbonate sequence related either to Sturtian (Babinski and Kaufman,
269 2003; Babinski et al., 2007; Vieira et al., 2007) or Marinoan (Caxito et al., 2012)
270 deglaciation. Despite a large suite of isotopic and chemostratigraphic data available
271 the depositional age has been unknown until recently. A Pb-Pb age of 740 ± 22 Ma
272 (**Fig. 4**) from basal carbonates of the Sete Lagoas Formation (Babinski et al., 2007)

was the first estimate for its depositional age. Subsequently, U-Pb detrital zircons in siliciclastics intervals provided maximum depositional ages of 610 Ma (Rodrigues, 2008) and 557 Ma (Paula-Santos, 2013) (**Fig. 4**). An Ediacaran fossil assemblage containing *Cloudina sp*. has recently been discovered in the central-eastern part of the basin (from the middle part of the Sete Lagoas Formation) (**Fig. 4**): this suggests a narrow time window (ca. 550-542 Ma) on account of the known global biozone that this assemblage represents (Warren et al., 2014 and references therein).

"Insert Figure 4 here"

From the above, it is clear that the depositional age of the Sete Lagoas Formation spans ca. 200 Myr. Thus, the different ages may imply that this formation contains a substantial hiatus within it. On the other hand, identical $^{87}Sr/^{86}Sr$ values (0.7074-0.7076) obtained both below and above the supposed unconformity separating the Cryogenian from the Ediacaran carbonates, argue against this hypothesis (Caxito et al., 2012).

In view of the uncertainties described earlier, and the necessity of understanding the context of deposition of the Bambuí Group, further provision of radiometric ages are required. In addition, most of the geochronological determinations derive from outcrops along the eastern margin of the basin (Babinski et al., 2007; Rodrigues, 2008; Paula-Santos, 2013). Thus, access to core material from the southwestern margin in the present study will extend knowledge to other parts of the carbonate platform.

3. Methods

299 *3.1 Sampling*

300 Samples of the 3 formations in this study were collected from proprietary drill cores
301 (**Fig. 1**). Drill cores intersecting the Paracatu and Serra do Garrote formations were
302 provided by Votorantim Mine and a mining company from the Arcos region supplied
303 the Sete Lagoas Formation samples. In the MASW03 (Paracatu Formation) core (**Fig.**
304 **5A**) the sampled interval spans 47.10 to 55.70 m (MD) and include dark grey to black
305 slates, with sporadic quartz as thin veins together with pyrite. VZCF001 (Serra do
306 Garrote Formation) core samples (**Fig. 5B**) extend from 280.10 to 292.65 m and
307 include black slates, with considerable carbonaceous material (staining). Pyrite is
308 present, both as lamina-parallel mineralization, and as crosscutting veins and
309 framboid nodules. Finally, LMR1009 (Sete Lagoas Formation) core samples (**Fig.**
310 **5C**) were obtained from four intervals; 1, from 36-47 m (microbial dolomite and
311 mudstones); 2, from 111-118 m (laminated limestones with carbonaceous seams); 3,
312 from 144-157 m (clay-rich limestones); 4, from 158-165 m (argillites). Following
313 Kendall et al. (2009a), ca. 100g samples were collected at 1 m intervals in each core.
314 Sub-sampling at further 0.4 m intervals was undertaken to detect further changes in
315 Re and Os abundance and isotope composition.

316 We note that petrographic inspection of the Serra do Garrote Formation in
317 core VZCF001 revealed faulting, brecciation of the host rock and pervasive quartz
318 veining. Care was taken to avoid these zones of hydrothermal alteration and
319 mineralization.

320

321 *3.2 Total organic carbon (TOC)*

322 TOC values for the all samples were determined at the School of Civil Engineering
323 and Geoscience of Newcastle University, UK. An accurately weighed 0.1 g of

powdered rock was digested in hot (60-70 °C) hydrochloric acid (4 mol/L) to remove the inorganic (carbonate) carbon. The decarbonated and washed samples (in deionised water) were then dried overnight in an oven at 65 °C. The organic carbon in the decarbonated samples was determined using a Leco CS230 Carbon-Sulphur analyser (previously calibrated on standard samples; standard deviation 3 %).

3.3 Re-Os geochronology

For Re-Os analysis, the core samples were polished using a diamond coated polishing pad to eliminate any metal contamination (e.g. cutting and drilling marks). Each sample was dried at 60 °C for 24 h and then crushed to a powder (c. 30 μm) in a zirconium dish using an automated shatterbox. Re and Os isotope analyses were carried out at Durham University's TOTAL laboratory for source rock geochronology and geochemistry at the Northern Centre for Isotopic and Elemental Tracing (NCIET) using methods outlined in Selby and Creaser (2003) and Selby (2007). Between 0.2 and 0.4 g of each sample was digested and equilibrated in a borosilicate carius tube in 8 ml of Cr^{VI}–H_2SO_4 together with a mixed tracer (spike) solution of ^{190}Os and ^{185}Re at 220 °C for 48 h. The Cr^{VI}–H_2SO_4 solution was used to liberate hydrogenous Re and Os, restricting the incorporation of non-hydrogenous Re and Os (Kendall et al., 2004). Solvent extraction ($CHCl_3$) for Re and Os purification, micro-distillation and anion chromatography methods were employed as outlined by Cumming et al. (2013). The purified Re and Os fractions were loaded onto Ni and Pt filaments, respectively (Selby, 2007), with the isotopic measurements determined by Negative Thermal Ionization Mass Spectrometry using a ThermoScientific mass spectrometer via static Faraday collection for Re and ion-counting using a secondary electron multiplier in peak-hopping mode for Os. Total procedural blanks during this study were 14.6 ±

0.16 pg and 0.05 ± 0.01 pg (1σ S.D., n = 3) for Re and Os, respectively, with an average $^{187}Os/^{188}Os$ value of 0.61 ± 0.03 (n = 3). Uncertainties for $^{187}Re/^{188}Os$ and $^{187}Os/^{188}Os$ were determined by error propagation of uncertainties in Re and Os mass spectrometer measurements, blank abundances and isotopic compositions, spike calibrations and reproducibility of standard Re and Os isotopic values. The Re–Os isotopic data including the 2σ calculated uncertainties for $^{187}Re/^{188}Os$ and $^{187}Os/^{188}Os$ and the associated error correlation function (rho) were regressed to yield a Re–Os date using Isoplot V. 4.0 and the λ ^{187}Re constant of 1.666×10^{-11} a^{-1} (Smoliar et al., 1996; Ludwig, 2003). The age uncertainty including the uncertainty of 0.35 % in the ^{187}Re decay constant only affects the third decimal place (Smoliar et al., 1996; Selby, 2007).

To evaluate mass spectrometry reproducibility, two in-house Re and Os (Durham Romil Osmium Standard=DROsS) solution standards were analyzed. The Re solution standard yields an average $^{185}Re/^{187}Re$ ratio of 0.598071 ± 0.001510 (1 S.D., n = 67), which is in agreement with the value reported for the AB-1 standard (Rooney et al., 2010). The measured difference in $^{185}Re/^{187}Re$ values for the Re standard solution and the accepted $^{185}Re/^{187}Re$ value (0.5974; Gramlich et al., 1973) is used to correct the measured sample Re isotope composition. The Os isotope reference solution (DROsS) gave an $^{187}Os/^{188}Os$ ratio of 0.160892 ± 0.000559 (1 S.D., n = 67), which is in agreement with previous studies (Rooney et al., 2010).

4. Results

4.1 TOC

The TOC results for all samples are presented in **Table 1** and **Fig. 5A, B and C**. The Sete Lagoas Formation has the lowest TOC of the 3 analyzed cores (<0.01 to 0.49

374 wt%), while the Serra do Garrote and Paracatu formations possess the highest TOC
375 values (0.75 to 2.12 wt % and 0.07 to 2.15 wt %, respectively). According to these
376 samples, the basin possesses fair quality as a potential hydrocarbon source rock, both
377 in carbonates and shales (c.f. Craig et al., 2013). Re-Os geochronology has been
378 applied successfully to rocks with < 0.5 % TOC (Kendall et al., 2004), thus this cut
379 off value was used to select the samples for Re-Os analysis. Only the samples from
380 the Paracatu and Serra do Garrote formations provided ≥1 wt% TOC (**Fig. 5A** and **B**),
381 in low-grade metamorphic rocks. Therefore, maturation analyses (Rock Eval) were
382 not performed.
383
384 "Insert Table 1 here"
385 "Insert Figure 5 here"
386
387 *4.2 Paracatu Slate Formation: Re-Os data*
388 The Paracatu Slate Formation samples have Re (0.3 – 4.1 ppb) and Os (53 – 297 ppt)
389 abundances (**Table 2**) that are close to or less than that of average continental crustal
390 values of 1 ppb and 50 ppt, respectively (Esser and Turekian, 1993; Peucker-
391 Ehrenbrink and Jahn, 2001; Hattori et al., 2003). The $^{187}Re/^{188}Os$ ratios display a
392 limited range from 24.2 to 79.6 and present-day $^{187}Os/^{188}Os$ ratios range from 0.667 to
393 1.593 (**Table 2**). Regression of the Re–Os isotope data yield a Re–Os age of 1002 ±
394 45 Ma (2σ, n = 4, Model 1, MSWD = 1.2, initial $^{187}Os/^{188}Os = 0.25 \pm 0.04$; **Fig. 6A**).
395 This initial $^{187}Os/^{188}Os$ (hereafter Os_i) value is remarkably unradiogenic and will be
396 discussed further in the following section.
397
398 "Insert Table 2 here"

"Insert Figure 6 here"

4.3 Serra do Garrote Formation: Re-Os data

The Serra do Garrote slates are enriched in Re (4 - 28 ppb) and Os (137 - 585 ppt; **Table 2**) and present a large spread in $^{187}Re/^{188}Os$ ratios (205.1 - 601.2) and $^{187}Os/^{188}Os$ ratios (3.628 - 12.207) (**Fig. 6B**). Replicate analysis of one Serra do Garrote sample (VZCF-6r) show good reproducibility in Re and Os abundances and $^{187}Re/^{188}Os$ and $^{187}Os/^{188}Os$ ratios. Contrary to the Paracatu Slate Formation, regression of the isotopic composition data for the Serra do Garrote Formation yield an imprecise, Model 3 age of 1304 ± 210 Ma (MSWD = 96), with a negative initial Os isotope value of -1.0 ± 1.4.

4.4 Sete Lagoas Formation: Re-Os data

The samples of the Sete Lagoas Formation have very low Re abundances <100 ppt, which are lower than estimated average (present-day) upper continental crust. These samples are not amenable to Re-Os geochronology as the low Re abundances would result in very large (>100 %) uncertainties in isotopic measurements using current analytical techniques.

5. Discussion

5.1 Paracatu Slate Formation

New Re–Os geochronology for the Paracatu Slate Formation yields a depositional age of 1002 ± 45 Ma, which agrees, within uncertainty, with U–Pb geochronology data (detrital zircons ca. 1040 Ma; Valeriano et al., 2004; Rodrigues et al., 2010; Dias, 2011). This relatively precise age represents the first successful application of the Re–

Os geochronometer in samples of the Canastra Group. The new Re–Os geochronology data adds credence to previous studies that suggest that there is no significant disturbance in the Re-Os systematics of carbonaceous organic-rich rocks that have experienced anhydrous greenschist facies metamorphism (Kendall et al., 2004; Rooney et al., 2011).

The Os_i value for seawater at the time of deposition of the Paracatu Formation (0.25 ± 0.04) is much less radiogenic than that of modern-day seawater (ca. 1.06; Levasseur et al., 1998) indicating that the dominant input of Os to seawater was non-radiogenic. This Os_i value is consistent with a marine Os budget dominated by extraterrestrial and ultramafic-mafic magmatic/hydrothermal inputs with minor contribution of radiogenic Os from continental weathering sources. The calculated Os isotope composition of continental crust at 1 Ga ranges from 0.5-1.0 thus indicating that this source played a minor role in the oceanic budget during this time as has been previously postulated (Kendall et al., 2009a; Rooney et al., 2010; van Acken et al., 2013). The Paracatu Slate Formation Os_i value provides an additional data point to the record for Precambrian seawater, evidencing that the change in global patterns of oxidative weathering and Os influx was of little importance, at least until the earliest Tonian (van Acken et al., 2013) although this remains contentious (Sperling et al., 2014).

Based on our Re-Os data, the Canastra Group was deposited at or around the Meso-Neoproterozoic boundary. This places the Canastra Group as a possible correlative of the Paranoá Group, considering the diagenetic xenotime U-Pb age of 1042 ± 22 Ma of the latter (Matteini et al., 2012). Moreover, the Re-Os age endorses tectonostratigraphic models of a passive margin sequence, deposited along the SW margin of the São Francisco-Congo paleocontinent (Pimentel et al., 2001, 2011;

449 Rodrigues et al., 2010). As the detrital zircons and depositional Re-Os isochron of the
450 Canastra Group are similar, this requires the rapid exhumation of the Mesoproterozoic
451 source region (main peak at ca. 1.2 Ga (Stenian); Rodrigues et al., 2010). On the other
452 hand, the youngest zircon population of the Paranoá Group interpreted as a maximum
453 depositional age (1540 Ma (Calymmian); Matteini et al., 2012) necessarily imposes
454 source isolation later in the evolution of the passive margin, if both units are indeed
455 chrono-correlatives.

456 Considering the amount of organic matter preserved even after maturation (ca.
457 2 wt %,), it is likely that the Paracatu Slate Formation of the Canastra Group
458 constituted an extensive hydrocarbon source rock. Despite no remaining potential for
459 further hydrocarbon generation, it is not implausible that between deposition (ca.
460 1000 Ma) and prior to the last tectono-metamorphic event recognised in the Brasília
461 Belt (ca. 600 Ma; Pimentel et al., 1999), the rock expelled hydrocarbons. However,
462 the presently available data is insufficient to determine the precise timing of
463 hydrocarbon generation/migration, as the intense deformation during the
464 Neoproterozoic Brasiliano Event and the posthumous erosion has obliterated true
465 stratigraphic thicknesses.

466

467 *5.2 Serra do Garrote Formation*

468 The Serra do Garrote Formation, which similarly to the Paracatu Formation has
469 experienced regional Brasiliano metamorphism (Dardenne, 2000), shows a large
470 scatter about the Re–Os regression line (Model 3, 1304 ± 210, MSWD = 96) together
471 with a negative initial Os isotope composition (-1.0 ± 1.4) suggestive of disturbances
472 to the Re–Os systematics. This imprecise age may result from either depositional
473 and/or post-depositional processes. The presence of detrital Os with variable

474 $^{187}Os/^{188}Os$ values, may result in imprecise and geologically meaningless ages
475 (Kendall et al., 2004, 2009a), but is considered an unlikely cause because the Cr^{VI}-
476 H_2SO_4 digestion technique preferentially liberates hydrogenous Os. Another feasible
477 cause of geological uncertainty for the Re-Os systematics may be variations in initial
478 Os isotope compositions during deposition (Selby and Creaser, 2003). In order to
479 avoid these heterogeneities, short stratigraphic sampling intervals (ca. 0.6 m) were
480 employed. The Os isotope composition of the Serra do Garrote Formation, however,
481 show variations that exceed those expected from temporal evolution in seawater
482 (unless sedimentation rates were anomalously low). Thus, these variations do not
483 fully account for the complex Re–Os systematics in the Serra do Garrote Formation.
484 Weathering and metamorphism are unlikely explanations for the scattered Re-
485 Os isotope systematics because drill core provided access to material showing no
486 apparent evidence of surficial alteration. Additionally, metamorphic conditions of the
487 Serra do Garrote Formation related to the Brasiliano Orogeny did not exceed
488 greenschist facies (Dardenne, 2000; Misi et al., 2005, 2007). Petrological evidence
489 (coarse pyrite aggregates, quartz veinlets and pervasive faulting and fracturing)
490 suggests the Serra do Garrote Formation has been affected by hydrothermal fluid
491 flow. Although we avoided sampling material with abundant quartz veins, the scatter
492 in the Re–Os regressions for the Serra do Garrote Formation and the Os_i signature of
493 the samples is indicative of a hydrothermal alteration origin, implying that there might
494 have been some mobilization of Re and Os by fluid flow. Similar Re-Os behaviour
495 has been observed by Rooney et al. (2011) for the Leny Limestone and by Kendall et
496 al. (2009b) for the Wollogorang Formation. Although the Vazante Ore hypogene
497 deposit is located in the overlying Serra do Poço Verde Formation (Monteiro et al.,
498 2006), we do not discount the possibility that the same mineralizing and oxidizing

499 fluids may have affected the Serra do Garrote Formation due to the proximity of well
500 VZCF001 to brecciated metadolomites and epigenetic willemitic ore bodies along the
501 Vazante Shear Zone (**Fig. 1B**). Therefore, it is possible that the high-temperature (>
502 250 °C), oxidizing and moderate saline (ca. 15 wt. % NaCl equiv.) brines that leached
503 base metals from the basement and ascended to finally interact with the host
504 dolostones of the Serra do Poço Verde (Monteiro et al., 2003; Misi et al., 2005) have
505 hydrated the Serra do Garrote slates, resulting in disturbance of the Re–Os
506 geochronometer. Similar alteration of Re-Os systematics by mineralizing fluid
507 circulation might also explain why previous attempts to date the Serra do Garrote and
508 Morro do Calcario formations with the Re-Os geochronometer (Geboy, 2006; Azmy
509 2008; Geboy et al., 2013) were unsuccessful.

510 It is likely that the extensive hydrothermal activity recorded in the Vazante
511 Group, and associated with the abundant Zn deposits (Monteiro et al., 2006) had
512 intrinsic relation with hydrocarbon generation, possibly sourced by the Serra do
513 Garrote Formation. Pyrobitumen has been observed within hydrothermal veins in the
514 carbonates of the overlying Morro do Calcário Formation (Rubo and Monteiro, 2010;
515 Tonietto, 2011) and hydrocarbon inclusions were described in sulfides of the Vazante
516 ore deposit (L. Monteiro *pers. comm*.). Future dating of these hydrocarbon products
517 with the ^{187}Re-^{187}Os radioisotope system (e.g., Selby and Creaser, 2005b) could help
518 constraining the timing of emplacement, the source of migrated hydrocarbons and the
519 temporal relation of the mineralization and hydrocarbon accumulation.

520

521 *5.3 Sete Lagoas Formation*

522 The low Re and Os abundance in the carbonate of the Sete Lagoas could be
523 intrinsically associated with the low TOC observed for the unit, and/or be directly

524 related to the depositional environment and the organic matter type (Colodner et al.,
525 1993; Crusius and Thomson, 2000; Selby and Creaser, 2003; Cumming et al., 2012;
526 Harris et al., 2013). Further, the observed low organic content can also be related to
527 thermal maturation (Peters and Cassa, 1994) which may cause a loss of 30-50 % of
528 the assumed original amount of TOC (Buchardt et al., 1986). Despite the intention of
529 accounting for the effects of maturation using biomarker studies, the results proved
530 inconclusive likely due to low volumes of organic matter analysed.

531 The recognition of palaeovalleys in outcrop (Martins-Ferreira et al., 2013),
532 and information of their infill with the Jequitaí Diamictites and post-glacial cap
533 Bambuí carbonate may have important implications for the distribution of organic-
534 rich facies. If indeed the Jequitaí glaciation left a sculpted palaeotopography, then
535 factors linked to restricted/open circulation within/out palaeovalleys may explain oxic
536 versus anoxic conditions for organic preservation and associated Re and Os
537 complexation. The lack of diamictites underlying carbonates of the Sete Lagoas
538 Formation in well LMR1009 (opposed to other cores of the region; F. Pimenta *pers.*
539 *comm*.; Kuchenbecker 2011; Kuchenbecker et al., 2011, 2013) could indicate a distal
540 position from paleodepressions, resulting in the low TOC values observed in this
541 particular location. This interpretation can only be tentative, however, because
542 seismic sections are not yet available in this region. Nevertheless, considering that
543 similar distributions are recognised in other Neoproterozoic post-glacial successions
544 (Bechstädt et al., 2009), and that organic-rich post-glacial facies in North Africa have
545 charged more than 50 major oil and gas fields (Lüning et al., 2000), the Sete Lagoas
546 Formation may yet have good source rock potential. Further studies are clearly
547 required to unravel the complex depositional history of this unit.
548

6. Conclusions

New Re–Os geochronology for the Paracatu Slate Formation yields a depositional age of 1002 ± 45 Ma and is in agreement, within uncertainty, of U–Pb detrital geochronology. This relatively precise age provides a more precise chronostratigraphic framework for understanding the tectonic evolution of the Canastra Group and the onset of sedimentation within the São Francisco Basin.

Disturbance of Re–Os systematics in the Serra do Garrote Formation is evident by an imprecise and inaccurate age along with a negative value for the Os_i value. These factors together with petrological evidence strongly suggest that the Re–Os system was disturbed in response to hydrothermal fluid flow, possibly associated with the Vazante ore deposit mineralization events. The circulation of oxygenated fluids through the Vazante Group is suggested to be the cause for disturbance to the Re-Os geochronometer. Consequently, care is necessary when applying the Re–Os deposition-age geochronometer to sedimentary rocks that have experienced tectonic deformation and hydrothermal fluid flow.

The lack of Re enrichment in the base of the Sete Lagoas Formation could be explained by the distribution of the organically-rich facies which, similarly to the deglacial shales in North Africa (Lüning et al., 2000), was inherited from glacial topography.

Acknowledgements

This research was generously funded by a grant from Sonangol to Daniel P. Le Heron, supporting the doctoral research of the first author and the AAPG Foundation Gordon I. Atwater Grant awarded to MEB. The Brazilian Council for Scientific and

574 Technological Development- CNPq provided a reaserch grant to F. F. Alkmim
575 (Grant#307531/2009-0). Votorantim mine and a mining company from Arcos region,
576 are thanked for provision of core samples and particular Samuel Boucas do Lago,
577 Gustavo Diniz Oliveira, Felipe Pimenta and Leonardo Lopes-Silva are thanked for
578 their assistance with the sample collection. Comments from two anonymous
579 reviewers greatly improved this paper.
580

581 **References**

582

583 Alkmim, F. F., and Martins-Neto, M. A., 2001. A Bacia intracratônica do São
584 Francisco: Arcabouço estrutural e cenários evolutivos. Bacia do São Francisco:
585 geologia e recursos naturais. SBG-MG, Belo Horizonte, 9-30.

586

587 Alkmim, F. F., Marshak, S., and Fonseca, M. A., 2001. Assembling West Gondwana
588 in the Neoproterozoic: clues from the São Francisco craton region, Brazil. Geology,
589 29(4), 319-322.

590

591 Alkmim, F. F., and Martins-Neto, M. A., 2012. Proterozoic first-order sedimentary
592 sequences of the São Francisco craton, eastern Brazil. Marine and Petroleum
593 Geology, 33(1), 127-139.

594

595 Almeida, F. F. M. D., Brito Neves, B. B. D., and Dal Ré Carneiro, C., 2000. The
596 origin and evolution of the South American Platform. Earth-Science Reviews, 50(1),
597 77-111.

598

599 Alvarenga, C. J. S., Della Giustina, M. E. S., Silva, M. G. C., Santos, R. V., Gioia, S.
600 M. C., Guimarães, E. M., Dardenne, M. A., Sial, A. N., Ferreira, V. P., 2007.
601 Variacões dos isótopos de C e Sr em carbonatos pré e pós-glaciacão Jequitaí
602 (Esturtiano) na região de Bezerra-Formosa, Goiás. Revista Brasileira de Geociências
603 37, 147-155.
604
605 Azmy, K., Kaufman, A. J., Misi, A., and Oliveira, T. F. D., 2006. Isotope stratigraphy
606 of the Lapa formation, São Francisco Basin, Brazil: implications for late
607 Neoproterozoic glacial events in South America. Precambrian Research, 149(3), 231-
608 248.
609
610 Azmy, K., Kendall, B., Creaser, R. A., Heaman, L., and de Oliveira, T. F., 2008.
611 Global correlation of the Vazante Group, São Francisco Basin, Brazil: Re–Os and U–
612 Pb radiometric age constraints. Precambrian Research, 164(3), 160-172.
613
614 Babinski, M., Kaufman, A. J., and Varni, M., 2003. First direct dating of a
615 Neoproterozoic post-glacial cap carbonate. South American Symposium on Isotope
616 Geology. 4, 321-323.
617
618 Babinski, M., Vieira, L. C., and Trindade, R. I., 2007. Direct dating of the Sete
619 Lagoas cap carbonate (Bambuí Group, Brazil) and implications for the
620 Neoproterozoic glacial events. Terra Nova, 19(6), 401-406.
621
622 Babinski, M., Pedrosa-Soares, A. C., Trindade, R. I. F., Martins, M., Noce, C. M., and
623 Liu, D., 2012. Neoproterozoic glacial deposits from the Araçuaí orogen, Brazil: Age,

624 provenance and correlations with the São Francisco craton and West Congo Belt.
625 Gondwana Research, 21(2), 451-465.
626
627 Bechstädt, T., Jäger, H., Spence, G. and Werner, G., 2009. Late Cryogenian
628 (Neoproterozoic) glacial and post-glacial successions at the southern margin of the
629 Congo Craton, northern Namibia: facies, palaeogeography and hydrocarbon
630 perspective. In: Craig, J., Thurow, J., Thusu, B., Whitham, A. and Abutarruma, Y.
631 (eds) Global Neoproterozoic Petroleum Systems: The Emerging Potential in North
632 Africa. Geological Society, London, Special Publications, 326, 255-287.
633
634 Buchardt, B., Clausen, J., and Thomsen, E., 1986. Carbon isotope composition of
635 Lower Palaeozoic kerogen: effects of maturation. Organic geochemistry, 10(1), 127-
636 134.
637
638 Caxito, F. D. A., Halverson, G. P., Uhlein, A., Stevenson, R., Gonçalves Dias, T., and
639 Uhlein, G. J., 2012. Marinoan glaciation in east central Brazil. Precambrian Research,
640 200, 38-58.
641
642 Chaves, M. L. D. S. C., Guimarães, J. T., and Andrade, K. W. 2010. Glaciomarine
643 lithofacies in the Jequitaí Formation: possible implications for the redistribution of
644 diamonds to the west of the Espinhaço Range (MG). Revista Brasileira de
645 Geociências, 40(4), 516-526.
646
647 Cohen, A. S., Coe, A. L., Bartlett, J. M., and Hawkesworth, C. J. 1999. Precise Re–Os
648 ages of organic-rich mudrocks and the Os isotope composition of Jurassic seawater.

649 Earth and Planetary Science Letters, 167(3), 159-173.
650
651 Colodner, D., Sachs, J., Ravizza, G., Turekian, K., Edmond, J and Boyle, E., 1993.
652 The geochemical cycle of rhenium: a reconnaissance. Earth and Planetary Science
653 Letters, **117,** 205-221.
654
655 Craig, J., Biffi, U., Galimberti, R. F., Ghori, K. A. R., Gorter, J. D., Hakhoo, N., Le
656 Heron, D. P., Thurow, J., Vecoli, M., 2013. The palaeobiology and geochemistry of
657 Precambrian hydrocarbon source rocks. Marine and Petroleum Geology, 40, 1-47.
658
659 Crusius, J., and Thomson, J., 2000. Comparative behavior of authigenic Re, U, and
660 Mo during reoxidation and subsequent long-term burial in marine sediments.
661 Geochimica et Cosmochimica Acta, **64,** 2233-2242.
662
663 Cukrov, N., De Alvarenga, C. J. S. and Uhlein, A., 2005. Litofácies da glaciação
664 Neoproterozóica nas porções sul do cráton do São Francisco: Exemplos de Jequitaí
665 (MG) e Cristalina (Go). Revista Brasileira de Geociências, 35, 69-76.
666
667 Cumming, V. M., Selby, D., and Lillis, P. G., 2012. Re–Os geochronology of the
668 lacustrine Green River Formation: Insights into direct depositional dating of
669 lacustrine successions, Re–Os systematics and paleocontinental weathering. Earth and
670 Planetary Science Letters, 359, 194-205.
671
672 Cumming, V.M, Poulton, S.W., Rooney, A.D. and Selby, D., 2013. Anoxia in the
673 terrestrial environment during the Late Mesoproterozoic. Geology 41(5), 583-586.

674

675 Dardenne, M. A., 1978. Síntese sobre a estratigrafia do Grupo Bambuí no Brasil
676 Central. SBG, Congresso Brassileiro de Geologia, 30, 507-610.

677

678 Dardenne, M. A., 2000. The Brasília fold Belt. In: Cordani, U. G., Milani, E. J.,
679 Thomaz Filho, A., Campos, D. A. (Eds.), Tectonic Evolution of South America. 31st
680 International Geological Congress, Rio de Janeiro, 231-263.

681

682 Dias, P. H. A., 2011. Estratigrafia dos grupos Canastra e Ibiá (Faixa Brasília
683 Meridional) na região de Ibiá, Minas Gerais: caracterização e estudo de proveniência
684 sedimentar com base em estudos isotópicos U-Pb e Sm-Nd. Master Thesis, Federal
685 University of Minas Gerais. Belo Horizonte, 92 p..

686

687 Esser, B. K., and Turekian, K. K., 1993. The osmium isotopic composition of the
688 continental crust. Geochimica et Cosmochimica Acta, 57(13), 3093-3104.

689

690 Freitas-Silva, F. H., 1996. Metalogênese do depósito do Morro do Ouro, Paracatu,
691 MG. Doctoral Thesis, University of Brasília. Brasília, 339 p..

692

693 Geboy, N. J., 2006. Rhenium-Osmium Age Determinations of Glaciogenic Shales
694 from the Mesoproterozoic Vazante Formation, Brazil. Master Thesis, Maryland
695 University. Maryland, 91 p..

696

697 Geboy, N. J., Kaufman, A. J., Walker, R. J., Misi, A., de Oliviera, T. F., Miller, K. E.,
698 Azmy, K., Kendall, B., and Poulton, S. W., 2013. Re–Os age constraints and new

699 observations of Proterozoic glacial deposits in the Vazante Group, Brazil.
700 Precambrian Research, 238, 199-213.
701
702 Georgiev, S., Stein, H. J., Hannah, J. L., Bingen, B., Weiss, H. M., and Piasecki, S.,
703 2011. Hot acidic Late Permian seas stifle life in record time. Earth and Planetary
704 Science Letters, 310(3), 389-400.
705
706 Gramlich, J. W., Murphy, T. J., Garner, E. L., Shields, W. R., 1973. Absolute isotopic
707 abundance ratio and atomic weight of a reference sample of rhenium. Journal of
708 Research of the National Bureau of Standards, 77A, 691–698.
709
710 Harris, N. B., Mnich, C. A., Selby, D., Korn, D., 2012. Minor and Trace Element and
711 Re-Os Chemistry of the Upper Devonian Woodford Shale, Permian Basin, West
712 Texas: Insights into Metal Abundance and Basin Processes. Chemical Geology, 356,
713 76-93.
714
715 Hattori, Y., Suzuki, K., Honda, M., and Shimizu, H., 2003. Re-Os isotope systematics
716 of the Taklimakan Desert sands, moraines and river sediments around the Taklimakan
717 Desert, and of Tibetan soils. Geochimica et cosmochimica acta, 67(6), 1203-1213.
718
719 Kendall B. S., Creaser R. A., Ross G. M. and Selby D., 2004. Constraints on the
720 timing of Marinoan ‘‘Snowball Earth” glaciation by ^{187}Re–^{187}Os dating of a
721 Neoproterozoic, post- glacial black shale in Western Canada. Earth Planetary Science
722 Letters 222, 729–740.
723

724 Kendall, B., Creaser, R. A., and Selby, D., 2009a. ^{187}Re-^{187}Os geochronology of
725 Precambrian organic-rich sedimentary rocks. Geological Society, London, Special
726 Publications, 326(1), 85-107.
727
728 Kendall, B., Creaser, R. A., Gordon, G. W., and Anbar, A. D. 2009b. Re–Os and Mo
729 isotope systematics of black shales from the Middle Proterozoic Velkerri and
730 Wollogorang formations, McArthur Basin, northern Australia. Geochimica et
731 Cosmochimica Acta, 73(9), 2534-2558.
732
733 Kuchenbecker, M., 2011. Quimioestratigrafia e proveniência sedimentar da porc¸ ão
734 basal do Grupo Bambuí em Arcos (MG). Master Thesis, Federal University of Minas
735 Gerais. Belo Horizonte, 91 p..
736
737 Kuchenbecker, M., Lopes-Silva, L., Pimenta, F., Pedrosa-Soares, A. C., and Babinski,
738 M., 2011. Estratigrafia da porção basal do grupo Bambuí na região de Arcos (MG):
739 uma contribuição a partir de testemunhos de sondagem. Geologia USP. Série
740 Científica, 11(2), 45-54.
741
742 Kuchenbecker, M., Babinski, M., Pedrosa-Soares, A. C., Costa, R. D. D., Lopes-
743 Silva, L., and Pimenta, F., 2013. Proveniência e análise sedimentar da porção basal do
744 Grupo Bambuí em Arcos (MG). Geologia USP. Série Científica, 13(4), 49-61.
745
746 Levasseur, S., Birck, J. L. and Allègre, C. J., 1998. Direct measurement of
747 femtomoles of osmium and the $^{187}Os/^{186}Os$ ratio in seawater. Science, 282(5387),
748 272-274.

749

750 Li, Z. X., Bogdanova, S. V., Collins, A. S., Davidson, A., De Waele, B., Ernst, R. E.,
751 Fitzsimons, I. C. W., Fuck R. A., Gladkochub, D. P., Jacobs, J., Karlstrom, K. E., Lu
752 S., Natapov, L. M., Pease, S. A., Pisarevsky, S. A., Thrane, K., and Vernikovsky, V.,
753 2008. Assembly, configuration, and break-up history of Rodinia: a synthesis.
754 Precambrian Research, 160(1), 179-210.

755

756 Ludwig, K., 2003. Isoplot/Ex, Version 3: A Geochronological Toolkit for Microsoft
757 Lüning, S., Craig, J., Loydell, D. K., Storch, P. and Fitches, W., 2000. Lowermost
758 Silurian 'hot shales' in north Africa and Arabia: regional distribution and depositional
759 model. Earth Science Reviews, 49, 121–200.

760

761 Macdonald, F. A., Schmitz, M. D., Crowley, J. L., Roots, C. F., Jones, D. S., Maloof,
762 A. C., Strauss, J. V., Cohen, P. A., Johnston, D. T., and Schrag, D. P., 2010.
763 Calibrating the Cryogenian. Science, 327(5970), 1241-1243.

764

765 Madalosso, A., 1980. Considerações sobre a paleogeografia do Grupo Bambuí na
766 região de Paracatu – Morro Agudo (MG). In: 31 Congresso Brasileiro de Geologia,
767 Anais, (2), 772-785.

768

769 Martins, M., and Lemos, V. B., 2007. Análise estratigráfica das seqüências
770 neoproterozóicas da Bacia do São Francisco. Brazilian Journal of Geology, 37(4),
771 156-167.

772

773 Martins-Ferreira, M. A., Campos, J. E. G. and Alvarenga, C. J. S. 2013. A Formação

774 Jequitaí na região de Vila Boa, GO: exemplo de sedimentação por geleiras terminais
775 no Neoproterozóico. Brazilian Journal of Geology, 43(2), 373-384.
776
777 Martins-Neto, M. A., 2009. Sequence stratigraphic framework of Proterozoic
778 successions in eastern Brazil. Marine and Petroleum Geology, 26(2), 163-176.
779
780 Matteini, M., Dantas, E. L., Pimentel, M. M., de Alvarenga, C. J. S., and Dardenne,
781 M. A., 2012. U–Pb and Hf isotope study on detrital zircons from the Paranoá Group,
782 Brasília Belt Brazil: Constraints on depositional age at Mesoproterozoic–
783 Neoproterozoic transition and tectono-magmatic events in the São Francisco craton.
784 Precambrian Research, 206, 168-181.
785
786 Misi, A., Iyer, S. S., Coelho, C. E. S., Tassinari, C. C. G., Franca-Rocha, W. J. S.,
787 Cunha, I. A., Gomes, A. S. R., Oliveira, T. F., Teixeira, J. B. G., Filho, V. M., 2005.
788 Sediment hosted lead–zinc deposits of the Neoproterozoic Bambuí Group and
789 correlative sequences, São Francisco Craton, Brazil: a review and a possible
790 metallogenic evolution model. Ore Geology Reviews 26, 263–304.
791
792 Misi, A., Kaufman, A. J., Veizer, J., Powis, K., Azmy, K., Boggiani, P. C., Gaucher,
793 C., Teixeira, J. B. G., Sanches, A. L., Iyer, S. S. S., 2007. Chemostratigraphic
794 correlation of Neoproterozoic successions in South America. Chemical Geology 237
795 (2007) 143–167.
796
797 Misi, A., Kaufman, A. J., Azmy, K., Dardenne, M. A., Sial, A. N., and de Oliveira, T.
798 F., 2011. Neoproterozoic successions of the São Francisco craton, Brazil: the Bambuí,

Una, Vazante and Vaza Barris/Miaba groups and their glaciogenic deposits. Geological Society, London, Memoirs, 36(1), 509-522.

Monteiro, L. V. S., Bettencourt, J. S., Bello, R. M. S., Juliani, C., Tassinari, C. C. G., Oliveira, T. F., and Pérez-Aguillar, A., 2003. Sulfur, carbon, oxygen and strontium isotopic evidences for the genesis of the hydrothermal zinc non-sulfide and sulfide mineralizations in the Vazante, Ambrosia and Fagundes deposits, MG, Brazil. In Short Papers IV South American Symposium on Isotope Geology, 748-751.

Monteiro, L. V. S., Bettencourt, J. S., Juliani, C., and de Oliveira, T. F., 2006. Geology, petrography, and mineral chemistry of the Vazante non-sulfide and Ambrósia and Fagundes sulfide-rich carbonate-hosted Zn–(Pb) deposits, Minas Gerais, Brazil. Ore Geology Reviews, 28(2), 201-234.

Olcott, A. N., Sessions, A. L., Corsetti, F. A., Kaufman, A. J., and De Oliviera, T. F., 2005. Biomarker evidence for photosynthesis during Neoproterozoic glaciation. Science, 310(5747), 471-474.

Paula-Santos, G.M., 2013. Quimioestratigrafia isotópica (C, O, Sr) e geocronologia (U-Pb, Sm-Nd) das rochas da Formação Sete Lagoas, Grupo Bambuí. Master Thesis, University of São Paulo. São Paulo, 142 p..

Pedrosa-Soares, A. C., Cordani, U. and Nutman, A., 2000. Constraining the age of Neoproterozoic glaciation in eastern Brazil: first U-Pb (SHRIMP) data from detritalzircons. Revista Brasileira de Geociências 30, 58-61.

824

825 Pereira, L. F., Dardenne, M. A., Rosière, C. A., and Pedrosa-Soares, A. C., 1994.
826 Evolução geológica dos grupos Canastra e Ibia na região entre Coromandel e Guarda-
827 Mor, MG. Revista Geonomos, 2(1), 22-32.

828

829 Peters, K. E., and Cassa, M. R., 1994. Applied source rock geochemistry. Memoirs-
830 American Association of Petroleum Geologists, 93-93.

831

832 Peucker-Ehrenbrink, B., and Jahn, B. M., 2001. Rhenium-osmium isotope systematics
833 and platinum group element concentrations: Loess and the upper continental crust.
834 Geochemistry, Geophysics, Geosystems, 2(10).

835

836 Pimentel, M. M., Fuck, R. A., and Botelho, N. F., 1999. Granites and the geodynamic
837 history of the Neoproterozoic Brasılia Belt, central Brazil: a review. Lithos, 46(3),
838 463-483.

839

840 Pimentel, M., Dardenne, M., Fuck, R., Viana, M., Junges, S. L., Fischel, D. P., Seer,
841 H.J., and Dantas, E. L., 2001. Nd isotopes and the provenance of detrital sediments of
842 the Neoproterozoic Brasılia Belt, central Brazil. Journal of South American Earth
843 Sciences, 14(6), 571-585.

844

845 Pimentel, M. M., Rodrigues, J. B., DellaGiustina, M. E. S., Junges, S., Matteini, M.,
846 and Armstrong, R., 2011. The tectonic evolution of the Neoproterozoic Brasília Belt,
847 central Brazil, based on SHRIMP and LA-ICPMS U–Pb sedimentary provenance
848 data: A review. Journal of South American Earth Sciences, 31(4), 345-357.

Ravizza, G., and Turekian, K. K., 1989. Application of the ^{187}Re-^{187}Os system to black shale geochronometry. Geochimica et Cosmochimica Acta, 53(12), 3257-3262.

Rodrigues, J. B., 2008. Proveniência de sedimentos dos grupos Canastra, Ibiá, Vazante e Bambuí e Um estudo de zircões detríticos e Idades Modelo Sm-Nd. Doctoral Thesis, University of Brasília. Brasília, 141 p..

Rodrigues, J. B., Pimentel, M. M., Dardenne, M. A., and Armstrong, R. A., 2010. Age, provenance and tectonic setting of the Canastra and Ibiá Groups (Brasília Belt, Brazil): Implications for the age of a Neoproterozoic glacial event in central Brazil. Journal of South American Earth Sciences, 29(2), 512-521.

Rodrigues, J. B., Pimentel, M. M., Buhn, B., Matteini, M., Dardenne, M. A., Alvarenga, C. J. S., and Armstrong, R. A., 2012. Provenance of the Vazante Group: New U–Pb, Sm–Nd, Lu–Hf isotopic data and implications for the tectonic evolution of the Neoproterozoic Brasília Belt. Gondwana Research, 21(2), 439-450.

Rooney, A. D., Selby, D., Houzay, J. P., and Renne, P. R., 2010. Re–Os geochronology of a Mesoproterozoic sedimentary succession, Taoudeni Basin, Mauritania: Implications for basin-wide correlations and Re–Os organic-rich sediments systematics. Earth and Planetary Science Letters, 289(3), 486-496.

Rooney, A. D., Chew, D. M., and Selby, D., 2011. Re–Os geochronology of the Neoproterozoic–Cambrian Dalradian supergroup of Scotland and Ireland:

874 implications for Neoproterozoic stratigraphy, glaciations and Re–Os systematics.
875 Precambrian Research, 185(3), 202-214.
876
877 Rooney, A. D., Macdonald, F. A., Strauss, J. V., Dudás, F. Ö., Hallmann, C., Selby,
878 D., 2014. Re-Os Geochronology and coupled Os-Sr isotope constraints on the Sturtian
879 snowball Earth. Proceedings of the National Academy of Sciences, 111, 51-56.
880
881 Rubo, R. A., and Monteiro, L. V. S., 2010. Sistemática de isótopos de oxigênio e
882 carbono aplicada ao estudo da evolução metalogenética do depósito de Zn-Pb de
883 Morro Agudo (MG). Brazilian Journal of Geology, 40(3), 438-452.
884
885 Santos, R. V., De Alvarenga, C. J. S., Dardenne, M. A., Sial, A. N., and Ferreira, V.
886 P., 2000. Carbon and oxygen isotope profiles across Meso-Neoproterozoic limestones
887 from central Brazil: Bambuí and Paranoá groups. Precambrian Research, 104(3), 107-
888 122.
889
890 Selby, D., and Creaser, R. A., 2003. Re–Os geochronology of organic rich sediments:
891 an evaluation of organic matter analysis methods. Chemical Geology, 200(3), 225-
892 240.
893
894 Selby, D., and Creaser, R. A., 2005a. Direct radiometric dating of the Devonian-
895 Mississippian time-scale boundary using the Re-Os black shale geochronometer.
896 Geology, 33(7), 545-548.
897
898 Selby, D., and Creaser, R. A., 2005b. Direct radiometric dating of hydrocarbon

899 deposits using rhenium-osmium isotopes. Science, 308(5726), 1293-1295.
900
901 Selby, D., Creaser, R. A., Dewing, K., and Fowler, M., 2005. Evaluation of bitumen
902 as a ^{187}Re–^{187}Os geochronometer for hydrocarbon maturation and migration: A test
903 case from the Polaris MVT deposit, Canada. Earth and Planetary Science Letters, 235
904 (1), 1-15.
905
906 Selby, D., 2007. Direct Rhenium-Osmium age of the Oxfordian-Kimmeridgian
907 boundary, Staffin bay, Isle of Skye, UK, and the Late Jurassic time scale. Norsk
908 Geologisk Tidsskrift, 87(3), 291-299.
909
910 Smoliar, M.I., Walker, R.J., Morgan, J.W., 1996. Re-Os isotope constraints on the age
911 of Group IIA, IIIA, IVA, and IVB iron meteorites. Science 271, 1099-1102.
912
913 Sperling, E.A., Rooney, A.D., Hays, L., Sergeev, V.N., Vorob'eva, N.G., Sergeeva,
914 N.D., Selby, D., Johnston, D.T., and Knoll, A.H., 2014. Redox heterogeneity of
915 subsurface waters in the Mesoproterozoic ocean. Geobiology.
916 DOI:10.1111/gbi.12091.
917
918 Tonietto, S. N., 2011. Diagênese e hidrotermalismo em rochas carbonáticas
919 proterozóicas: Grupos Bambuí e Vazante, Bacia do São Francisco. Master Thesis.
920 University of Brasília. Brasília, 196 p..
921
922 Uhlein, A., Trompette, R. R., Egydio-Silva, M., Vauhez, M., 2007. A glaciação
923 Sturtiana (~750 Ma), a estrutura do rifte Macaúbas Santo Onofre e a estratigrafia do

924 Grupo Macaúbas, Faixa Araçuaí. Revista Geonomos, 15, 45-60.
925
926 Valeriano, C. M., Machado, N., Simonetti, A., Valladares, C. S., Seer, H. J., Simões,
927 L. S. A., 2004. U-Pb geochronology of the Southern Brasília Belt (SE-BRAZIL):
928 sedimentary provenance, Neoproterozoic Orogeny and assembly of West Gondwana.
929 Precambrian Research 130, 27-55.
930
931 Valeriano, C. M., Pimentel, M. M., Heilbron, M., Almeida, J. C. H., Trouw, R. A. J.,
932 2008. Tectonic evolution of the Brasília Belt, central Brazil, and early assembly of
933 Gondwana. In: Pankhurst, R.J., Trouw, R.A.J., Brito Neves, B.B., De Wit, M.J.
934 (Eds.), West Gondwana: Pre-cenozoic Correlations across the South Atlantic Region.
935 Geological Society, London, Special Publications, 294, 197-210.
936
937 van Acken, D., Thomson, D., Rainbird, R. H., and Creaser, R. A., 2013. Constraining
938 the depositional history of the Neoproterozoic Shaler Supergroup, Amundsen Basin,
939 NW Canada: Rhenium-osmium dating of black shales from the Wynniatt and Boot
940 Inlet Formations. Precambrian Research, 236, 124-131.
941
942 Vieira, L. C., Almeida, R. P., Trindade, R. I., Nogueira, A. C., and Janikian, L., 2007.
943 A Formação Sete Lagoas em sua área-tipo: fácies, estratigrafia e sistemas
944 deposicionais. Revista Brasileira de Geociências, 37 (4), 1-14.
945
946 Warren, L. V., Quaglio, F., Riccomini, C., Simões, M. G., Poiré, D. G., Strikis, N. M.,
947 Anelli L.E., and Strikis, P. C., 2014. The puzzle assembled: Ediacaran guide fossil
948 Cloudina reveals an old proto-Gondwana seaway. Geology, 42(5), 391-394.

949

950 Zalán, P. V., and Silva, P. C. R., 2007. Bacia do São Francisco. Boletim de

951 Geociências da Petrobrás, 15(2), 561-571.

952 **Figure Captions**

953

954 Fig. 1. Location and geology of the study area. (A) São Francisco Craton, São
955 Francisco Basin and surrounding belts (BFB=Brasilia Fold Belt); (B) Simplified
956 geological map of the Brasília Belt (after Dardenne, 2000).

957

958 Fig. 2. Lithostratigraphic column of the Canastra Group (modified from Dardenne,
959 2000). Youngest concordant age interpreted as maximum depositional age:
960 [(1)]Rodrigues et al. (2010); [(2)]Dias, 2011; [(3)] Valeriano (2004). Average thickness from
961 Pereira et al. (1994).

962

963 Fig. 3. Lithostratigraphic column of the Vazante Group (modified from Dardenne,
964 2000). Youngest concordant age interpreted as maximum depositional age:
965 [(1)]Rodrigues et al. (2012); Re-Os isochron interpreted as depositional age: [(2)]Geboy
966 (2006); [(3)]Azmy et al. (2008); [(4)]Geboy et al. (2013). Average thickness from Misi et
967 al. (2011).

968

969 Fig. 4. Lithostratigraphic column of the Bambuí Group (modified from Dardenne,
970 2000). Youngest concordant age interpreted as maximum depositional age:
971 [(1)]Rodrigues (2008); [(3)]Paula-Santos (2013). Pb-Pb isochron interpreted as
972 depositional age: [(2)]Babinski et al. (2007). Index fossil *Cloudina*: [(4)]Warren et al.
973 (2014). Average thickness from Vieira et al. (2007).

974

975 Fig. 5. Stratigraphic levels used for TOC and Re–Os measurements (A) Paracatu
976 Formation, drillhole MASW03; (B) Serra do Garrote Formation, drillcore VZCF001;

977 (C) Sete Lagoas Formation, drillcore LMR1009.

978

979 Fig. 6. Re–Os isochron diagram (A) Paracatu Formation organic-rich slates, drillhole
980 MASW03; (B) Serra do Garrote Formation organic-rich slates, drillhole VZCF001.

981

982

983 **Tables**

984

985 *Table 1*: TOC content for the Canastra, Vazante and Bambuí groups.

986

987 *Table 2*: Re-Os isotope data for the Paracatu and Serra do Garrote formations. *Rho is
988 the associated error correlation at 2σ (Ludwig, 1980). $^{\S}Os_i$ is the initial $^{187}Os/^{188}Os$
989 isotope ratio calculated at 1002 Ma for the Paracatu Formation and 1300 Ma for the
990 Serra do Garrote Formation. VZCF-6r is a repeat analysis and was not included in the
991 regression

992

Sample	Re (ppb)	±	Os	±	$^{187}Re/^{188}Os$	±	$^{187}Os/^{188}Os$	±	Rho*	Osi§
Paracatú										
MASW03-36	0.30	0.001	64.8	1.2	24.2	0.3	0.667	0.038	0.705	0.260
MASW03-38	0.36	0.001	52.7	1.0	36.1	0.7	0.847	0.030	0.705	0.239
MASW03-40	4.11	0.013	296.5	2.1	79.6	0.8	1.593	0.040	0.656	0.253
MASW03-42	1.31	0.004	175.1	1.0	39.8	0.6	0.934	0.030	0.654	0.264
Serra do Garrote										
VZCF001-6	18.7	0.06	507.2	5.2	317.9	2.8	6.167	0.070	0.656	-0.793
VZCF001-6r	18.9	0.06	515.7	9.3	314.3	6.4	6.136	0.174	0.698	-0.746
VZCF001-11	9.2	0.03	260.2	2.5	269.9	2.4	4.654	0.053	0.657	-1.255
VZCF001-13	28.3	0.09	584.6	7.0	601.2	5.2	12.207	0.139	0.656	-0.956
VZCF001-3	4.0	0.01	136.8	2.2	205.1	4.2	3.628	0.103	0.699	-0.862

Formation	Sample	Depth [m]	TOC [wt%]
Serra do Garrote	VZCF001-1	280.23	0.85
	VZCF001-2	281.33	1.53
	VZCF001-3	281.55	0.07
	VZCF001-4	281.78	2.15
	VZCF001-5	282.00	0.87
	VZCF001-6	282.23	2.10
	VZCF001-7	285.78	0.72
	VZCF001-8	286.63	0.20
	VZCF001-9	287.78	0.93
	VZCF001-10	288.43	1.48
	VZCF001-11	288.98	0.62
	VZCF001-12	289.15	1.98
	VZCF001-13	289.60	1.50
	VZCF001-14	289.98	1.38
	VZCF001-15	292.55	1.89
Paracatú	MASW03-33	47.6	2.12
	MASW03-34	48.0	1.76
	MASW03-35	48.3	1.75
	MASW03-36	48.6	1.56
	MASW03-37	49.9	1.48
	MASW03-38	50.4	1.03
	MASW03-39	50.7	1.42
	MASW03-40	51.0	0.92
	MASW03-41	52.3	1.23
	MASW03-42	52.6	1.19
	MASW03-43	52.9	1.16
	MASW03-44	53.2	0.99
	MASW03-45	53.5	1.59
	MASW03-46	55.6	0.75
	MASW03-47	55.9	1.13
Sete Lagoas	LIMR1009-U4S15	35.85	0.08
	LIMR1009-U4S14	36.85	0.17
	LIMR1009-U4S13	37.85	0.03
	LIMR1009-U4S12	38.85	0.05
	LIMR1009-U4S11	39.85	0.02
	LIMR1009-U4S10	40.85	0.04
	LIMR1009-U4S9	41.85	0.02
	LIMR1009-U4S8	42.85	0.04
	LIMR1009-U4S7	43.85	0.10
	LIMR1009-U4S6	44.85	0.03
	LIMR1009-U4S5	45.85	0.04
	LIMR1009-U4S4	46.25	0.02
	LIMR1009-U4S3	46.65	0.01
	LIMR1009-U4S2	47.05	0.02
	LIMR1009-U4S1	47.57	0.01
	LIMR1009-U3S8	112.34	0.01
	LIMR1009-U3S7	113.34	0.01
	LIMR1009-U3S6	114.34	0.02
	LIMR1009-U3S5	115.34	0.08
	LIMR1009-U3S4	116.34	0.01
	LIMR1009-U3S3	116.74	0.04
	LIMR1009-U3S2	117.14	0.03
	LIMR1009-U3S1	117.54	0.02
	LIMR1009-U2S15	145.75	0.00
	LIMR1009-U2S14	146.75	0.00
	LIMR1009-U2S13	147.75	0.00
	LIMR1009-U2S12	148.75	0.02
	LIMR1009-U2S11	149.75	0.00
	LIMR1009-U2S10	150.75	0.02
	LIMR1009-U2S9	151.75	0.08
	LIMR1009-U2S8	152.75	0.00

	LIMR1009-U2S7	153.75	0.01
	LIMR1009-U2S6	154.75	0.01
	LIMR1009-U2S5	155.75	0.00
	LIMR1009-U2S4	156.15	0.01
	LIMR1009-U2S3	156.55	0.06
	LIMR1009-U2S2	156.95	0.02
	LIMR1009-U2S1	157.35	0.13
	LIMR1009-U1S1	158.15	0.32
	LIMR1009-U1S2	158.55	0.22
	LIMR1009-U1S3	158.95	0.24
	LIMR1009-U1S4	159.35	0.24
	LIMR1009-U1S5	159.75	0.22
	LIMR1009-U1S6	160.75	0.06
	LIMR1009-U1S7	161.75	0.36
	LIMR1009-U1S8	162.75	0.14
	LIMR1009-U1S9	163.75	0.49
	LIMR1009-U1S10	164.75	0.33

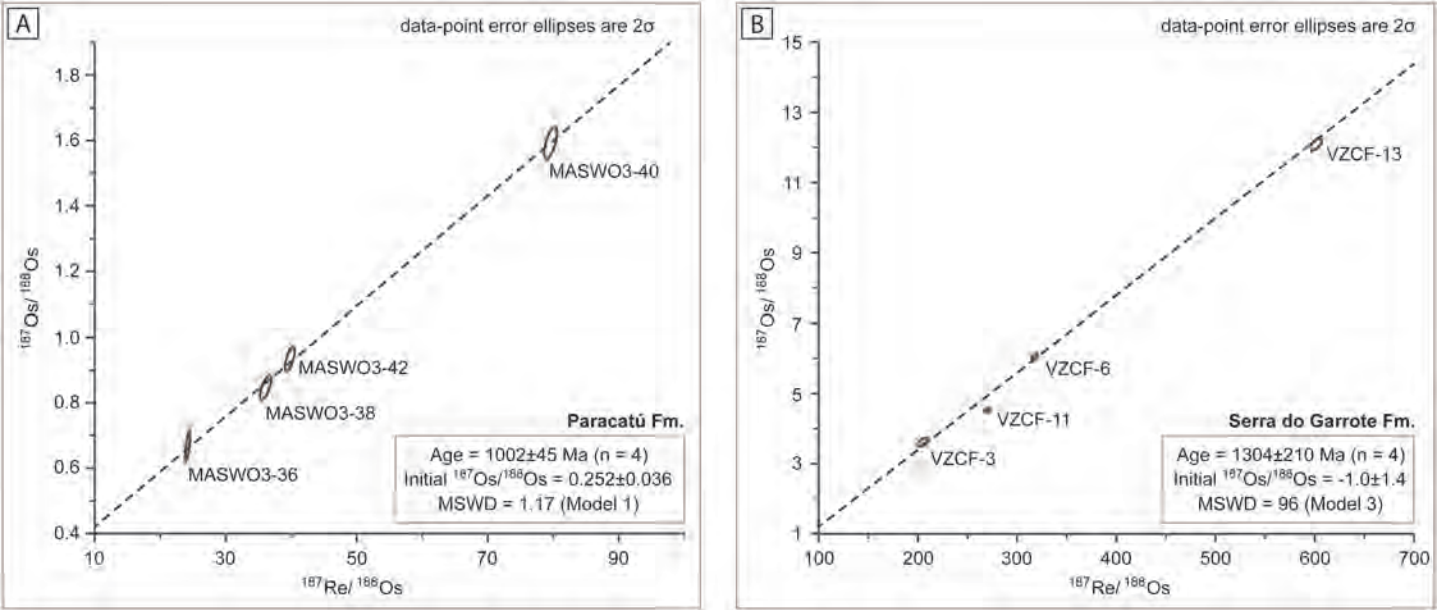
A
data-point error ellipses are 2σ
MASWO3-40
MASWO3-42
MASWO3-38
MASWO3-36
Paracatú Fm.
Age = 1002±45 Ma (n = 4)
Initial 187Os/188Os = 0.252±0.036
MSWD = 1.17 (Model 1)
187Os/188Os
187Re/188Os
B
data-point error ellipses are 2σ
VZCF-13
VZCF-6
VZCF-11
VZCF-3
Serra do Garrote Fm.
Age = 1304±210 Ma (n = 4)
Initial 187Os/188Os = -1.0±1.4
MSWD = 96 (Model 3)
187Os/188Os
187Re/188Os

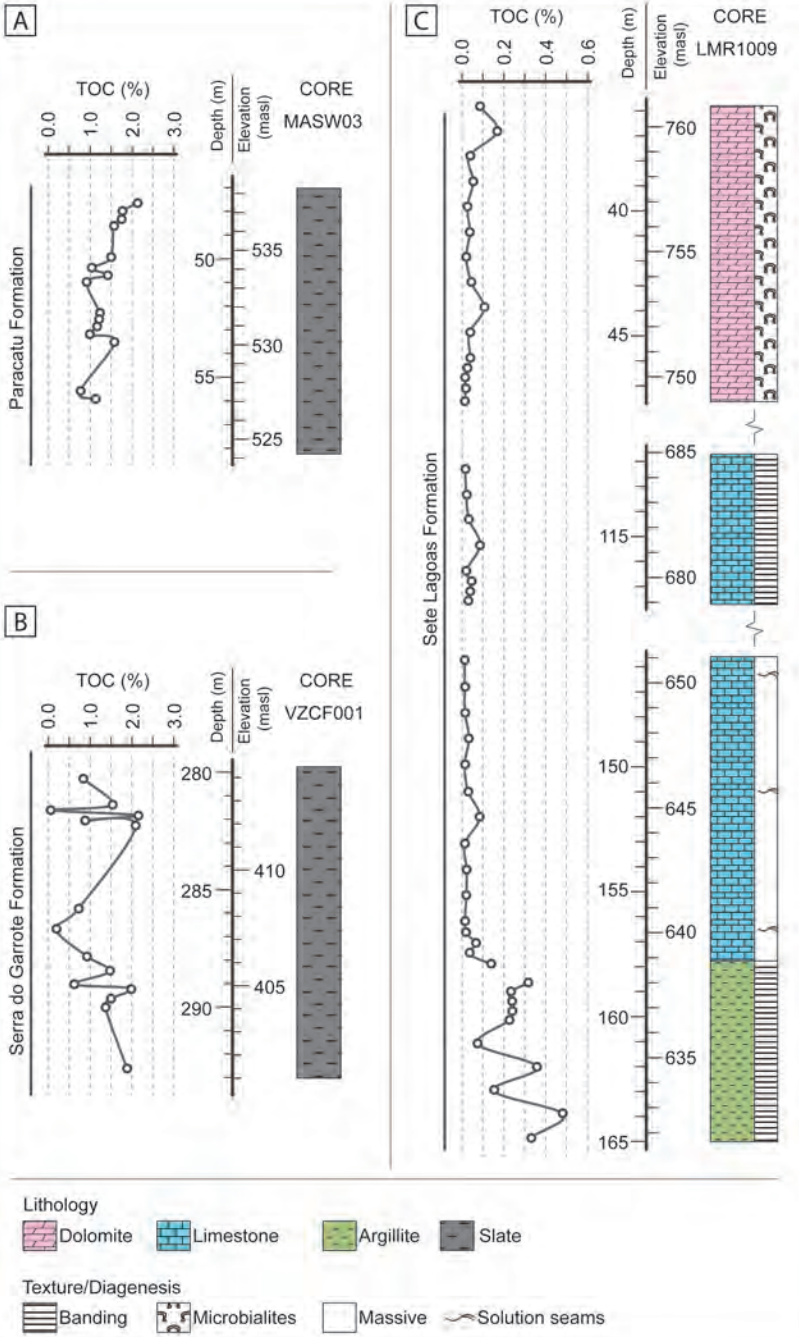
A
TOC (%)
0.0
1.0
2.0
3.0
Depth (m)
Elevation (masl)
CORE
MASW03
Paracatu Formation
50
55
535
530
525
B
TOC (%)
0.0
1.0
2.0
3.0
Depth (m)
Elevation (masl)
CORE
VZCF001
Serra do Garrote Formation
280
285
290
410
405
C
TOC (%)
0.0
0.2
0.4
0.6
Depth (m)
Elevation (masl)
CORE
LMR1009
Sete Lagoas Formation
760
40
755
45
750
685
115
680
650
150
645
155
640
160
635
165
Lithology
Dolomite
Limestone
Argillite
Slate
Texture/Diagenesis
Banding
Microbialites
Massive
Solution seams

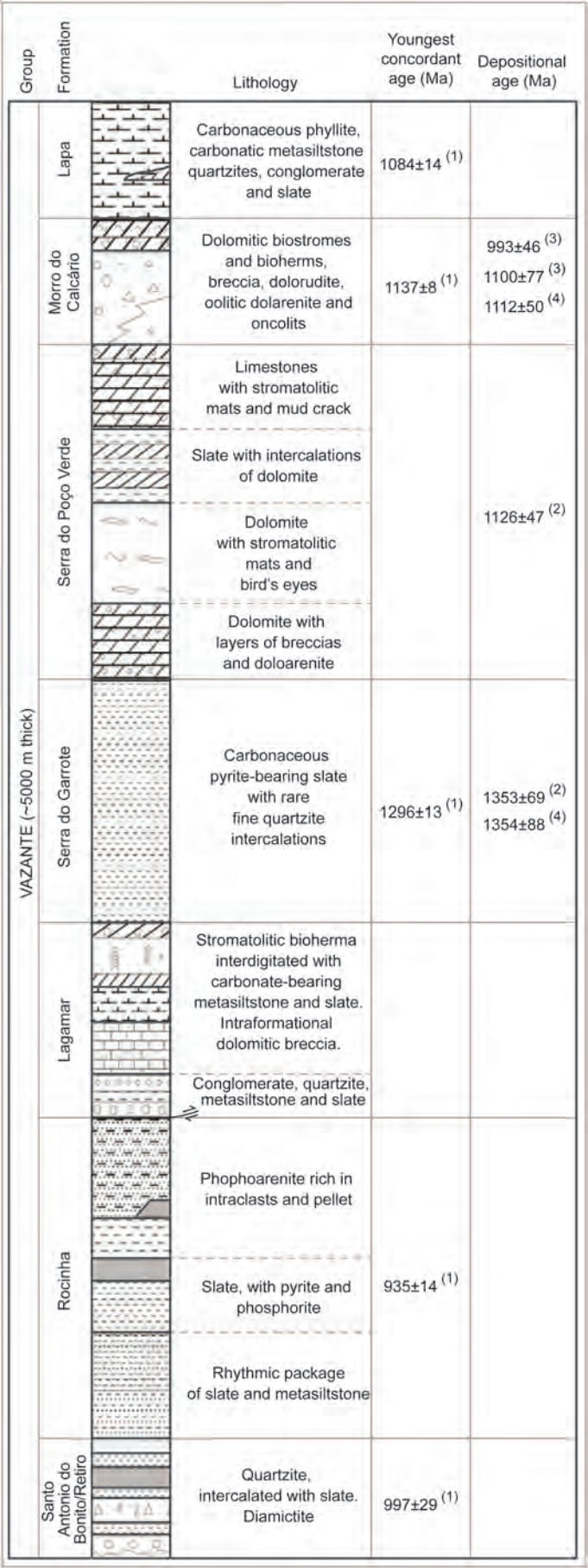
Group
Formation
Lithology
Youngest concordant age (Ma)
Depositional age (Ma)
VAZANTE (~5000 m thick)
Lapa
Carbonaceous phyllite, carbonatic metasiltstone quartzites, conglomerate and slate
1084±14 (1)
Morro do Calcário
Dolomitic biostromes and bioherms, breccia, dolorudite, oolitic dolarenite and oncolits
1137±8 (1)
993±46 (3)
1100±77 (3)
1112±50 (4)
Serra do Poço Verde
Limestones with stromatolitic mats and mud crack
Slate with intercalations of dolomite
Dolomite with stromatolitic mats and bird's eyes
Dolomite with layers of breccias and doloarenite
1126±47 (2)
Serra do Garrote
Carbonaceous pyrite-bearing slate with rare fine quartzite intercalations
1296±13 (1)
1353±69 (2)
1354±88 (4)
Lagamar
Stromatolitic bioherma interdigitated with carbonate-bearing metasiltstone and slate. Intraformational dolomitic breccia.
Conglomerate, quartzite, metasiltstone and slate
Rocinha
Phophoarenite rich in intraclasts and pellet
Slate, with pyrite and phosphorite
935±14 (1)
Rhythmic package of slate and metasiltstone
Santo Antonio do Bonito/Retiro
Quartzite, intercalated with slate. Diamictite
997±29 (1)

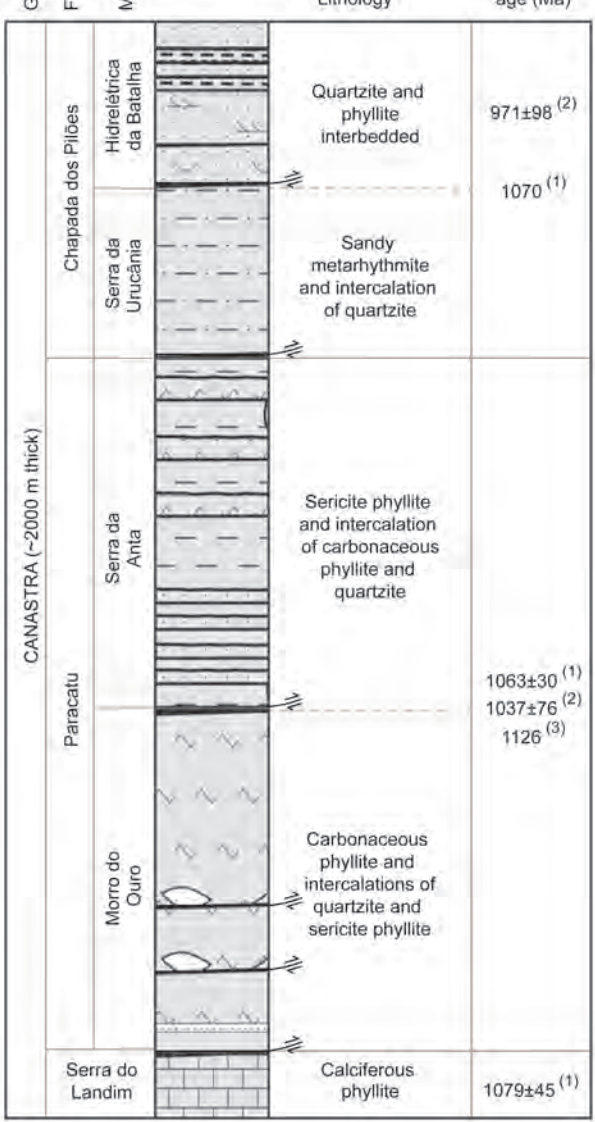
Group
Formation
Member
Lithology
Youngest concordant age (Ma)
CANASTRA (~2000 m thick)
Paracatu
Chapada dos Pilões
Hidrelétrica da Batalha
Serra da Urucânia
Serra da Anta
Morro do Ouro
Serra do Landim
Quartzite and phyllite interbedded
Sandy metarhythmite and intercalation of quartzite
Sericite phyllite and intercalation of carbonaceous phyllite and quartzite
Carbonaceous phyllite and intercalations of quartzite and sericite phyllite
Calciferous phyllite
971±98 (2)
1070 (1)
1063±30 (1)
1037±76 (2)
1126 (3)
1079±45 (1)

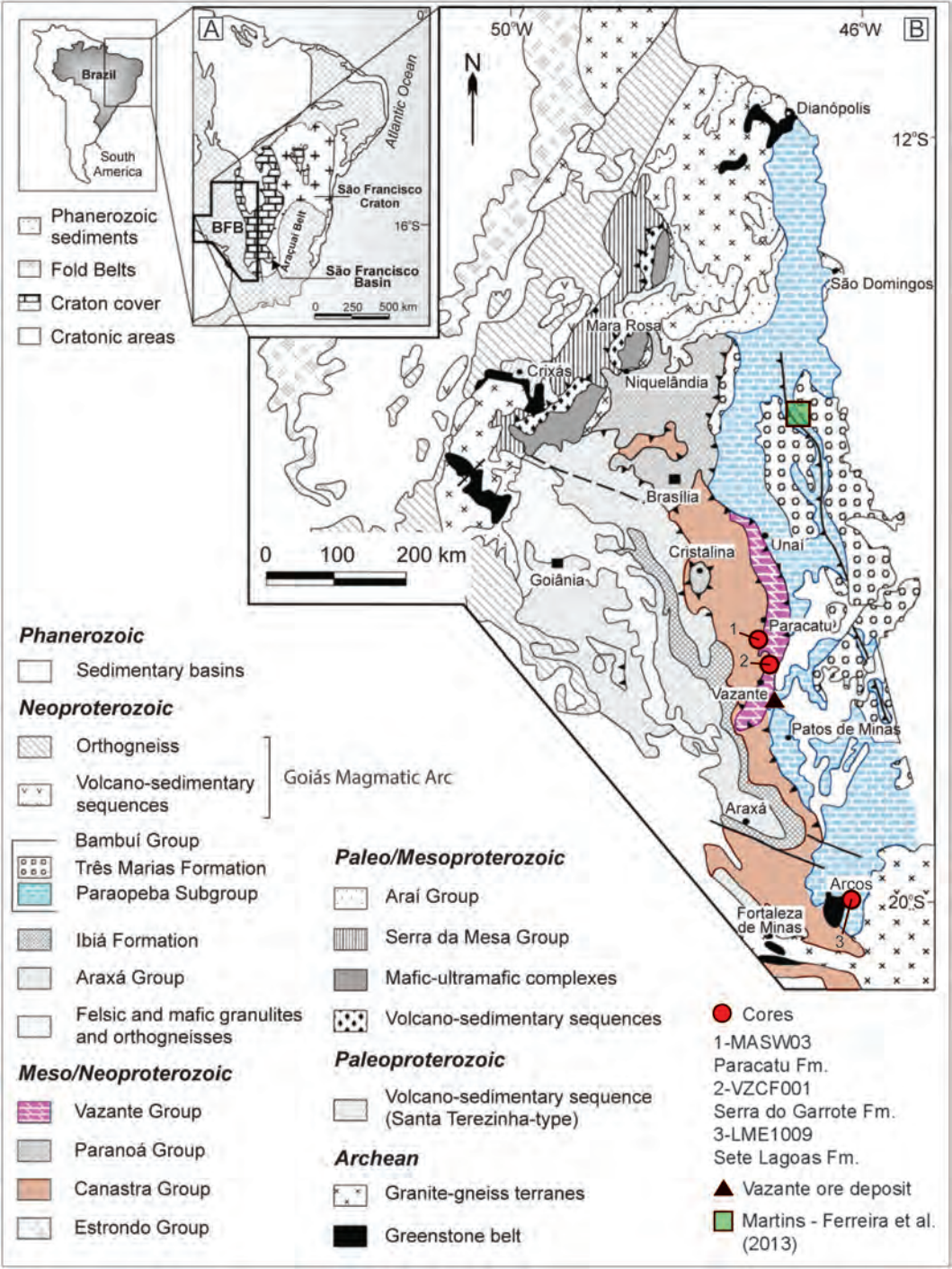
Brazil
South America
A
B
Atlantic Ocean
São Francisco Craton
BFB
Araçuaí Belt
São Francisco Basin
16°S
0 250 500 km
50°W
46°W
N
12°S
20°S
Dianópolis
São Domingos
Mara Rosa
Crixás
Niquelândia
Brasília
Cristalina
Unaí
Goiânia
Paracatu
Vazante
Patos de Minas
Araxá
Arcos
Fortaleza de Minas
0 100 200 km
Phanerozoic sediments
Fold Belts
Craton cover
Cratonic areas
Phanerozoic
Sedimentary basins
Neoproterozoic
Orthogneiss
Volcano-sedimentary sequences
Goiás Magmatic Arc
Bambuí Group
Três Marias Formation
Paraopeba Subgroup
Ibiá Formation
Araxá Group
Felsic and mafic granulites and orthogneisses
Meso/Neoproterozoic
Vazante Group
Paranoá Group
Canastra Group
Estrondo Group
Paleo/Mesoproterozoic
Araí Group
Serra da Mesa Group
Mafic-ultramafic complexes
Volcano-sedimentary sequences
Paleoproterozoic
Volcano-sedimentary sequence (Santa Terezinha-type)
Archean
Granite-gneiss terranes
Greenstone belt
Cores
1-MASW03
Paracatu Fm.
2-VZCF001
Serra do Garrote Fm.
3-LME1009
Sete Lagoas Fm.
Vazante ore deposit
Martins - Ferreira et al. (2013)